

DIPARTIMENTO DI MATEMATICA
“Francesco Brioschi”
POLITECNICO DI MILANO

**In vitro tissue growth: a multiscale
computational model of the
dynamically evolving biophysical
environment**

Causin, P.; Sacco, R.; Verri, M.

Collezione dei *Quaderni di Dipartimento*, numero **QDD 109**
Inserito negli *Archivi Digitali di Dipartimento* in data 6-10-2011



Piazza Leonardo da Vinci, 32 - 20133 Milano (Italy)

In vitro tissue growth: a multiscale computational model of the dynamically evolving biophysical environment

Paola Causin ^a, Riccardo Sacco ^b, Maurizio Verri ^b

^a*Dipartimento di Matematica “F. Enriques”, Università degli Studi di Milano
via Saldini 50, 20133 Milano, Italy*

^b*Dipartimento di Matematica “F. Brioschi”, Politecnico di Milano
piazza Leonardo da Vinci 32, 20133 Milano, Italy*

Abstract

Tissue Engineering (TE) is a field at the crossroad between Medicine, Life Sciences and Engineering, aimed at understanding the principles of tissue growth, and applying them to produce biologically functional replacements for clinical use. To achieve such an ambitious goal, complex biophysical phenomena must be mastered and related to the appropriate environment (nutrient delivery, fluid-mechanical loading and structural support) to be provided to cells. The TE problem is inherently multiphysics/multiscale, as it is characterized by material heterogeneities and interplaying processes occurring within a wide range of temporal and spatial scales. The concept we pursue in this paper is to use computational modelling of the TE problem to gain a quantitative and comprehensive understanding of phenomena often difficult to be accessed experimentally. The present model represents, to our knowledge, the first example of a self-consistent high-resolution description of coupled nutrient mass transport, fluid-dynamics and biomass production in TE constructs. We specifically focus on articular cartilage regeneration based on dynamically perfused bioreactors and we investigate three issues critical in this application. First, we study oxygen distribution in the construct, since achieving an optimal level throughout the construct is a main tool to improve tissue quality. Second, we provide a quantitative evaluation on how interstitial perfusion can enhance nutrient delivery and, ultimately, biomass production, compared to static culture. Third, we perform a sensitivity analysis with respect to biophysical parameters related to matrix production, assessing their role in tissue regeneration.

Key words: Tissue engineering, multiscale model, mass transfer in heterogeneous media, model of biomass synthesis, interstitial perfusion bioreactor.

1 Introduction

In vitro cultivation of functional tissues for body repair, the so-called “Tissue Engineering”, is investigated as a promising technique able to improve life conditions of millions of patients worldwide (see, *e.g.*, [22,39,1]). Yet, at present, to bridge the gap between being a concept and a clinical applicable procedure, a definite need arises for improved control over the functional properties and composition of the cultivated tissue.

A major application of TE is found in the regeneration of articular cartilage, a tissue with very poor capabilities of self repair. Portions of cartilage tissue have been grown in bioreactors starting from donor chondrocyte cells attached to polymeric scaffolds in mixed flasks, rotating wall or direct perfusion bioreactors [11,25,37]. Cells, initially seeded so to yield a quasi uniform thin layer on the scaffold walls [40], undergo a first period of rapid proliferation during the early culture time (5–7 days), after which they secrete (2–4 weeks) the typical highly hydrated matrix comprising proteoglycan monomers assembled with GAGs anchored to hyaluronic acid chains and collagen [30,11]. In order to ensure cell viability and efficient metabolic activity, a properly tuned level of nutrients must be delivered to cells. This is not an easy task, since nutrient mass transfer is significantly limited by the progressive obstruction of the scaffold due to biomass growth [28,11]. Direct perfusion bioreactors have been shown to be able to deliver more efficiently nutrient to cells and for this reason they are the reference devices in this work. The specific experimental setting we consider (described in detail in [33,32]), consists in scaffolds with average porosity 77%, interstitially perfused by the culture medium through a pumping system. The medium flow rate at the inlet is kept constant overall the experiment and the flow direction is inverted cyclically every 40 minutes. The presence of an interstitial flow has the side effect of introducing further mechanical and biophysical processes which must be as well analyzed and mastered.

This paper stems from the concept that an advanced computational model can significantly help in gaining knowledge in this complex scenario, giving access to pieces of information that are experimentally difficult or impossible to obtain. The biophysical phenomena occurring during *in vitro* tissue regeneration encompass a wide range of embedded scales. Fig. 1 shows five distinct scales at which (at least) the considered problem can be modeled. Several computational models in literature focus on the *Macroscale*. These studies numerically evaluate the fluid-dynamical field and/or the nutrient profile in the construct as if the system were *tout court* homogeneous [28,29,9], or use homogenized approaches including effective transport parameters [41,6,36]. Even if adopting the Macroscale perspective provides a significant insight on the overall performance of the bioreactor, the actual local distribution of the

fields of interest remains unknown. A change of perspective implies to zoom down to the smaller scales, entering the microscopic behavior of the system, an approach strongly motivated by recent improvement of experimental measurements based on micro-imaging techniques, which provide high-resolution time-continuous data [38]. CFD models of interstitially perfused bioreactors coupled with oxygen mass transport equations solved in microdomains composed of a few pores, corresponding to the *Mesoscale*, have been proposed in [33,31]. The problem is solved on realistic configurations as well as on idealized simplified geometries. In both cases, the CFD analysis is carried out on the uncellularized scaffold, that is, completely neglecting the presence of the growing biomass. An improvement to this latter approach is obtained in [23] where CFD computations are performed on a series of different “frozen” simplified geometries representing the pattern of deposition of the biomass extracted from experimental images at the pore size for different time levels.

A first attempt for including multiple scales in a mathematical model of TE can be found in [7], where an axial symmetric model is solved at the Macroscale to compute boundary conditions which are used to drive the solution of a 3D CFD model in a Microscale domain constituted by the uncellularized scaffold geometry. In this model, no feedback from the Microscale model to the Macroscale model was introduced. In the present article, we construct a genuine multiscale/multiphysics model characterized by:

- a self-consistent coupling among nutrient distribution, cell metabolic activity and geometry evolution;
- a biophysical description of biomass evolution;
- a structure of modular sub-blocks, whose modelling/computational complexity can be properly tuned to the problem at hand without affecting the overall structure;
- an affordable computational cost;
- the possibility of a direct integration with experimental data obtained from microscopical images of histological sections of tissue engineered constructs.

With the aid of such a model, we investigate in three distinct studies the coupled phenomena of nutrient mass transfer and biomass growth. A first study stems from the observation that cartilage cells are *in vivo* physiologically subjected to low levels of oxygen tension (p_{O_2} ranging from 2 to 10%), but a widespread practice in TE is to supply “hyper-physiological” conditions ($p_{O_2} = 20\%$) at the bioreactor inlet [17,8]. We carry out simulations to relate a given inlet nutrient concentration with the time evolution of the corresponding distribution inside the construct and we explore how inlet concentration can be tuned to optimize local oxygenation levels. In a second study, we investigate the effect of perfusion on nutrient mass transfer. Perfusion, enhancing nutrient delivery, allows for a more uniform development of biomass across the construct thickness. This results, in general, in a shorter culture time to reach

a certain biomass production level with respect to the static case. However, our simulations show that, while the transient behavior to reach steady-state is significantly different from static culture conditions, the final level of oxygen is definitely influenced by diffusion barriers. Eventually, in a third study, we further assess the role of diffusion barriers, carrying out a sensitivity analysis on the biomass production rate and extracellular matrix inhibition effect with respect to biomass growth. The general conclusion of this analysis is that diffusion barriers always play against, but, due to the nonlinear nature of the problem at hand, there are some combinations of the design and biophysical parameters which are more favorable than others in ultimately improving the bioreactor performance.

2 Mathematical Model

We consider the typical configuration of a disc-shaped scaffold consisting of the union of interconnected scaffold pores, culture medium and biomass. We let \mathbf{x} be the coordinate vector, t the time variable and $I_t := [t_{start}, t_{end}]$ the temporal interval of engineered tissue cultivation, t_{start} and t_{end} being the starting and final culture times. Fig. 2 shows the construct geometry and introduces the corresponding notation used throughout the paper.

2.1 Full Scale Analysis

The full scale approach we advocate in this work consists of the coupled solution for every $t \in I_t$ of the following differential systems.

Fluid Subdomain Model

- a) advection–diffusion problem for nutrient concentration $c = c(\mathbf{x}, t)$ in Ω_{fl} :

$$\begin{cases} \frac{\partial c}{\partial t} + \nabla \cdot \mathbf{J} = 0, \\ \mathbf{J} = -D_{fl} \nabla c + \mathbf{v}c, \end{cases} \quad (1)$$

where \mathbf{v} is the fluid velocity determined by system (2), \mathbf{J} is the nutrient mass flux and D_{fl} is the nutrient diffusivity in the fluid phase.

The equation system (1) is supplied with the initial condition $c(\mathbf{x}, 0) = c_0$ and the boundary conditions $c = c_0$ on $\partial\Omega_{fl} \cap \partial\Omega_{in}$ and $\mathbf{J} \cdot \mathbf{n} = 0$ on $\partial\Omega_{fl} \cap \partial\Omega_l$ and on $\partial\Omega_{fl} \cap \partial\Omega_{sc}$, where c_0 is the (constant) inlet nutrient concentration.

- b) Navier–Stokes equations [21] for fluid velocity $\mathbf{v} = \mathbf{v}(\mathbf{x}, t)$ and fluid pressure $p = p(\mathbf{x}, t)$ in Ω_{fl} :

$$\begin{cases} \nabla \cdot \mathbf{v} = 0, \\ \rho_{fl} \left[\frac{\partial \mathbf{v}}{\partial t} + (\mathbf{v} \cdot \nabla) \mathbf{v} \right] = -\nabla p + \mu_{fl} \Delta \mathbf{v}, \end{cases} \quad (2)$$

where ρ_{fl} and μ_{fl} are the density and the dynamic viscosity of the medium, respectively.

The equation system (2) is supplied with the initial condition $\mathbf{v}(\mathbf{x}, 0) = \mathbf{0}$ and the boundary conditions $\mathbf{v} = \mathbf{v}_{in}$ on $\partial\Omega_{fl} \cap \partial\Omega_{in}$, $\mathbf{v} = \mathbf{0}$ on $\partial\Omega_{fl} \cap \partial\Omega_{sc}$, and $\partial\mathbf{v}/\partial\mathbf{n} = \mathbf{0}$ on $\partial\Omega_{fl} \cap \partial\Omega_l$.

Biomass Subdomain Model

- a) diffusion–reaction problem for nutrient concentration $c = c(\mathbf{x}, t)$ in Ω_b :

$$\begin{cases} \frac{\partial c}{\partial t} + \nabla \cdot \mathbf{J} = Q \\ \mathbf{J} = -D_b \nabla c, \end{cases} \quad (3)$$

where D_b is the nutrient diffusivity in the biomass phase and the function $Q = Q(c)$ represents mass consumption due to cellular metabolism, expressed by the Michaelis–Menten kinetics

$$Q = -\frac{Rc}{K_{1/2} + c}, \quad (4)$$

where $R = \Psi_{max} \xi_{cells}$, ξ_{cells} being the number of cells per unit biomass volume and Ψ_{max} the maximal nutrient consumption rate, respectively, while $K_{1/2}$ is the half saturation constant. The equation system (3) is supplied with the initial condition $c(\mathbf{x}, 0) = c_0$ and the boundary conditions $c = c_0$ on $\partial\Omega_b \cap \partial\Omega_{in}$ and $\mathbf{J} \cdot \mathbf{n} = 0$ on $\partial\Omega_b \cap \partial\Omega_l$ and on $\partial\Omega_b \cap \partial\Omega_{sc}$;

- b) model for fluid velocity: $\mathbf{v} = \mathbf{0}$ in Ω_b ;
c) model for biomass growth:

$$\Omega_b = \Omega_b(t; c, \mathbf{v}|_{\partial\Omega_{fl} \cap \partial\Omega_b}, \text{other biophysical parameters}). \quad (5)$$

Fluid-Biomass Interface Model

At the fluid-biomass interface, the following conditions must be satisfied:

$$c|_{\partial\Omega_b} = \kappa c|_{\partial\Omega_{fl}}, \quad \mathbf{J}|_{\partial\Omega_{fl}} \cdot \mathbf{n} = \mathbf{J}|_{\partial\Omega_b} \cdot \mathbf{n}, \quad \mathbf{v}|_{\partial\Omega_{fl}} = \mathbf{0}. \quad (6)$$

The first condition expresses local mass equilibrium, with positive constant $\kappa \leq 1$ [43]; the second condition represents mass flux continuity and the third condition is the standard adherence of a fluid at a solid wall.

We will refer in the following to the above coupled system of equations as the 3D Full Scale (3DFS) model.

Modeling assumptions

The following assumptions in the mathematical description of engineered tissue growth will be adopted in the present work.

1) Nutrient mass transfer can be described by a sequence of quasi-stationary steps, because the time scale of nutrient transport is much faster than biomass growth [29,36]. This corresponds to neglecting the term $\partial c/\partial t$ in Eqns. (1)₁ and Eqns. (3)₁. Notice that the temporal dependence of the fields c and \mathbf{v} is however retained through the coupling with biomass growth.

2) The left-hand side of (2)₂ can be neglected because the Reynolds number of the fluid-dynamical problem is very small. For example, assuming an inlet velocity $|\mathbf{v}_{in}| = 50 \mu\text{ms}^{-1}$, a scaffold porosity of 77% [34] and $L = 1\text{mm}$ [36], we have that the microscopic Reynolds number (*i.e.*, computed at the pore size scale) is of the order of $5 \cdot 10^{-4}$, while the macroscopic Reynolds number (*i.e.*, computed at bioreactor scale) is of the order of $6 \cdot 10^{-2}$.

3) Biomass growth is described according to the fact that, after seeding, cells undergo a first proliferative phase, followed by an intense phase of ECM secretion. Since proliferation is a time-limited but highly complex mechanism, which should deserve on its own an accurate modeling work, we limit ourselves to consider here a “post-initial” condition where cells have already reached their maximal number N_{cells}^{tot} (see [29,27] for a similar approach). Moreover, we consider cells and biomass to have the same mass density ρ_b , which will be assumed to be equal to the clear fluid density ρ_{fl} .

Idealized geometry

A realistic geometry of the construct can be extracted from μ -CT data and used, upon segmentation and post-processing, for simulations. Since this is not the focus of this work, we rather consider the idealized geometry shown in Fig. 3A, referred to the experimental setting of [32] and already numerically investigated by several authors [34,7,23]. The simplified bioreactor domain is described by a regular mosaic of “cubic pores” (Fig. 3A,B), obtained intersecting a cube of size $2b$ with a sphere of diameter larger than the pore side. Letting then $V_{\text{cub}} = (2b)^3$ the volume of the cubic pore, we define the construct design porosity Φ_0 as the ratio between the initial void volume and V_{cub} .

2.2 Multiscale Model

Even with the introduction of the above simplifications, the computational challenge of solving the 3DFS model is still a too demanding task even for the more advanced numerical techniques and powerful machine resources. This difficulty is principally represented by the need of using a very high scale resolution, say, up to the Microscale/Cellular scale, further complicated by the presence of internal moving boundaries due to biomass growth. A change of modelling perspective is thus required. The idea we pursue in this work is to use a scale separation argument and localize the 3DFS model at two distinct–but interacting–scales, the Macro and Micro scales. At the Macroscale level, a homogenized form of the 3DFS model is used for the gross characterization of internal fields and inclusion of technological input parameters, while at the Microscale level a decoupled solution of the 3DFS model is carried out on disjoint computational domains of strongly reduced size for the characterization of fine biomass growth phenomena and direct interaction with high–resolution experimental measurements. The two scales are coupled and interact through bridging variables, which for Micro to Macro transition represent effective–averaged parameters, while for Macro to Micro transition represent appropriate boundary conditions.

To mathematically identify in the rest of the paper each of the two scale levels introduced above, we will denote by the subscripts m and M quantities and operators defined at the Microscale and Macroscale, and by (m, M) and (M, m) quantities obtained from Micro to Macro and Macro to Micro scale transitions, as described below.

The Microscale Model

The Microscale model is formulated at a characteristic size corresponding to the functional sub–unit constituted by the single pore. Despite the strong size reduction with respect to the 3DFS problem, the difficulty of computationally handling moving interfaces in a 3D domain remains unsolved. A possible escape to this difficulty relies on the experimental evidence that biomass growth mainly occurs in the void spherical space symmetrically along the pore radial direction [23]. This suggests to introduce in the mathematical description of Microscale phenomena the assumption of *spherical symmetry*. With this assumption the intrinsic 3D nature of the biomass growth is maintained at the benefit of a drastic reduction of computational complexity because all problem variables depend only on the radial coordinate. To work under this hypothesis, we introduce an “equivalent spherical pore” (Fig. 3C) consisting of a sphere of radius r_w whose volume $V_w = 4\pi r_w^3/3$ is equal to the void volume of the pore, which yields $r_w = b(6\Phi_0/\pi)^{1/3}$. The spherical pore is adopted as the computational domain Ω_m , and is composed of the union of the time-varying fluid

and biomass micro-regions $\Omega_{m,fl}$ and $\Omega_{m,b}$ (Fig. 3C). The origin of the radial system is located at the centroid \mathbf{x}_P of the considered pore P . To simplify the notation, the dependence on \mathbf{x}_P of all the quantities in the Microscale model will be understood, if not otherwise specified.

The 3DFS model localized at the Microscale level amounts to solving the following coupled differential sub-systems for every $t \in I_t$:

- a) model for Microscale nutrient concentration $c_m = c_m(r, t)$:
- 1) in the Microscale fluid subdomain $\Omega_{m,fl}$: $c_m = c_{(M,m)}$, where $c_{(M,m)}$ is the Macro-Micro scale bridging concentration computed as described in *SI Methods*.
 - 2) in the Microscale biomass subdomain $\Omega_{m,b}$:

$$\begin{cases} \frac{1}{r^2} \frac{\partial(r^2 J_m(c_m))}{\partial r} = Q(c_m), \\ J_m(c_m) = -D_b \frac{\partial c_m}{\partial r}. \end{cases} \quad (7)$$

The equation system (7) is supplied with the following interface and boundary conditions:

$$\begin{aligned} c_m &= \kappa c_{(M,m)} & \text{at } r = r_b, \\ J_m(c_m) &= 0 & \text{at } r = r_w. \end{aligned} \quad (8)$$

- b) model for the radial component of the Microscale fluid velocity $v_m = v_m(r, t)$:
- 1) in the Microscale fluid subdomain $\Omega_{m,fl}$: the only admissible spherically symmetric solution of the Stokes equation

$$v_m = \alpha/r^2, \quad (9)$$

where $\alpha = \alpha(t)$ is a function to be determined enforcing the continuity of the nutrient flux at $r = r_b$, that is

$$\frac{\alpha}{r_b^2} c_{(M,m)} = J_m(c_m) \Big|_{r=r_b}. \quad (10)$$

Notice that condition (10) establishes a constraint between the radial component of the velocity at the fluid–biomass interface and the interface position itself.

- 2) in the Microscale biomass subdomain $\Omega_{m,b}$:
 $v_m = 0$.

c) model for biomass radial thickness and interface displacement:

secretion of biomass from cells causes the medium–biomass interface to move due to the increase of the width of the region $\Omega_{m,b}$ at the expense of a reduction of $\Omega_{m,fl}$. In radial symmetry, the biomass region is identified by the evolution of the quantity $h_b := r_w - r_b$, which represents the time dependent thickness of the biomass and consists of cells and accumulated extracellular matrix.

Before describing the model in detail, we need to establish some notation and fundamental relationships. Let $V_b = V_b(t) = V_w - 4\pi(r_w - h_b(t))^3/3$ denote the volume occupied by the biomass in the spherical pore at time t . Then, the amount of biomass present at time t in pore P is $m_b(t) = \rho_b V_b(t)$. We assume the biomass at time $t = 0$ to be purely composed of a layer of N_{cells}^{tot} cells - which according to the previous assumption on the “post–initial” condition is a fixed given value - forming an equivalent annular region of thickness h_0 , so that $m_b(0) = \rho_b(V_w - 4\pi(r_w - h_0)^3/3)$.

To monitor biomass secretion, we follow the standard experimental and theoretical practice of choosing GAG as a marker of ECM accumulation. For modeling simplicity, we focus only on the evolution of the GAG “bound” fraction (see also [42]); we refer to [10,19] for a more general and detailed description including unbound, bound and degraded GAG fractions. Denoting by $m_{GAG} = m_{GAG}(t)$ the GAG mass contained at time t in $\Omega_{m,b}$, we assume the following 0D lumped model of the GAG synthesis process [29,27]:

$$\begin{cases} \frac{dm_{GAG}}{dt} = k_{GAG} \xi_{cells} \bar{c}_m \left(1 - \frac{m_{GAG}}{m_{GAG,inh}}\right) \\ m_{GAG}(0) = 0, \end{cases} \quad (11)$$

where k_{GAG} is the GAG synthesis rate, $\xi_{cells}(t) = N_{cells}^{tot}/V_b(t)$ the time-dependent volumetric density of cells secreting biomass, and $\bar{c}_m = \bar{c}_m(t)$ the average Microscale nutrient concentration in the biomass. Product inhibition is taken into account by including the right-hand side in (11)₁ dependence on a saturation GAG level $m_{GAG,inh}$. This term represents in a simplified way the inhibitory feedback effect exerted by cell surface hyaluronan receptors and integrins in the assembly of the matrix, which “sense” the location and quantity of GAG and collagen and send messages to maintain homeostatic concentrations [20]. To close the problem, we need to connect the GAG mass production to the whole biomass amount. With this aim, we assume the following constitutive relation

$$m_b(t) = m_b(0) + E m_{GAG}(t), \quad (12)$$

where the parameter $E > 1$ keeps into account the fact that the natural cartilagineous ECM is composed for the 70-80% of its wet weight

of water, while in the remaining fraction of the wet weight the 10-15% are collagen fibrils and the 5% are GAG components, respectively [5]. Upon solving problem (11) supplied with Eq. (12), we get the following functional relation between the biomass thickness and the secreted GAG mass:

$$\begin{cases} \frac{h_b(t)}{r_w} := 1 - y(t), \\ y(0) = 1 - h_0/r_w, \\ y(t) = y(0) \sqrt[3]{1 - \frac{E m_{GAG}(t)}{\rho_b V_w (y(0))^3}}, \end{cases} \quad (13)$$

where $y(t)$ represents the normalized radius of the fluid domain. Relation (13)₃ shows that $y(t)$ is a decreasing function of the accumulated GAG mass (and hence $h_b(t)$ an increasing function). Since $y(t)$ must be a non-negative quantity, this implies the following upper bound on the GAG mass that can be accumulated due to sole geometrical restrictions

$$0 \leq m_{GAG}(t) \leq \frac{\rho_b V_w}{E} \left(1 - \frac{h_0}{r_w}\right)^3 := m_{GAG*} \quad \forall t \geq 0.$$

At the same time, contact inhibition effects included in model (11) imply that $m_{GAG}(t) \leq m_{GAG,inh}$, $\forall t \geq 0$. Putting together the two bounds, we obtain that the maximum theoretical value of the biomass thickness, denoted by $h_{b,max}$, is given by

$$h_{b,max} = r_w \min \left(1, 1 - \left(1 - \frac{h_0}{r_w} \right) \sqrt[3]{1 - \frac{m_{GAG,inh}}{m_{GAG*}}} \right). \quad (14)$$

The Macroscale Model

The Macroscale problem is formulated in the idealized bioreactor domain $\Omega_M \equiv \Omega$ shown in Fig. 3A. The main modeling assumption to reduce the complexity of the 3DFS model is to consider a homogenized continuum version of the corresponding equations, that is uniformly valid in the whole domain Ω_M . To further reduce the computational cost, we also assume that nutrient mass transport across neighboring pores in the (y, z) plane can be neglected and that boundary effects on the lateral walls of the construct can be ignored as well. Let us denote by \mathcal{P}_H the collection of N_L cubic pores P of size $2b$ that constitute an ordered stack composing Ω_M : due to the above hypothesis, the stack is a 1D (x -dependent) domain, over which solutions requiring a low computational effort will be sought. Moreover, even if each stack has in principle its own dynamics, in the present device configuration it is reasonable to assume that all the pores located in the same (y, z) plane are indistinguishable, *i.e.*, they are supplied with the same amount of nutrient and they exhibit the same cellular metabolic activity, so that they have the same bio-physical

behavior. The global bioreactor behavior is thus the overall contribution of the parallel of the N_S indistinguishable stacks. Moreover, because of the periodically alternating direction of the medium inlet velocity, we can assume the concentration profile to be a symmetric function with respect to $x = L/2 := \ell$. All the above hypotheses are supported by our computational experience with multi-dimensional numerical simulations [36] and by several other simulations reported in the literature (see, *e.g.*, [7]).

The 3DFS model localized at the Macroscale level amounts to solving in Ω_M the following coupled differential sub-systems for every $t \in I_t$:

a) model for nutrient concentration $c_M = c_M(x, t)$:

$$\begin{cases} \frac{\partial J_M(c_M)}{\partial x} = Q_M(c_M), \\ J_M(c_M) = -D_{(m,M)} \frac{\partial c_M}{\partial x} + v_M c_M, \end{cases} \quad (15)$$

where v_M is the Macroscale velocity field determined from system (16) and $Q_M(c_M) = R_{(m,M)}c_M/(K_{1/2} + c_M)$. The coefficients $D_{(m,M)}$ and $R_{(m,M)}$ are the *effective* nutrient diffusivity and consumption rate, respectively, computed as described in *SI Methods*. The equation system (15) is supplied by the boundary conditions $c_M = c_0$ at $x = 0$ and $-D_{(m,M)} \frac{\partial c_M}{\partial x} = 0$ at $x = \ell$. This latter condition expresses the symmetry of the concentration profile at $x = \ell$.

b) Darcy model for fluid velocity $v_M = v_M(x, t)$ and piezometric head $p_M = p_M(x, t)$:

$$\begin{cases} \frac{\partial v_M}{\partial x} = 0, \\ -\frac{\partial p_M}{\partial x} + B_M = 0, \\ B_M = -\frac{\mu_{fl} \Phi_{(m,M)}}{K_{(m,M)}(\Phi_{(m,M)})} v_M, \end{cases} \quad (16)$$

where $K_{(m,M)}$ is the effective hydraulic permeability, computed as described in *SI Methods*. The equation system (16) is the 1D homogenized macroscale version of the Navier–Stokes system (2) under the assumption of neglecting inertial terms (see [18] for a complete derivation). The body force term B_M represents the total drag force per unit volume exerted on the perfusion fluid particles by the scaffold/biomass component of the bioreactor. The equation system (16) is supplied by the boundary conditions $p_M = p_0$ at $x = 0$ and $p_M = 0$ at $x = \ell$. The boundary term p_0 is

determined by enforcing the global balance

$$-\frac{p_M(\ell) - p_M(0)}{\ell} = \frac{p_0}{\ell} = \frac{\mu_{fl} \Phi_0}{K_{(m,M)}(\Phi_0)} v_{in}.$$

- c) biomass growth: included through the effective coefficients obtained from Micro to Macro scale bridging.

2.3 Computational Algorithm

We partition the time interval I_t into $N_t \geq 1$ subintervals $I_{t,n} := [t_n, t_{n+1}]$ of uniform width $\Delta t = I_t/N_t$, in such a way that $t_n = t_{start} + n\Delta t$, $n = 0, \dots, N_t - 1$. For any function $f = f(\mathbf{x}, t)$, we set $f^n := f(\mathbf{x}, t_n)$. At each time level t_{n+1} , $n = 0, \dots, N_t - 1$, the Microscale and Macroscale problems are solved in sequence in a staggered fashion. Moreover, both the Microscale and Macroscale sub-systems are internally linearized. The resulting computational algorithm is shown in Fig. 4. Details on the solution of the sub-problems appearing in Fig. 4 are given in *SI Methods*.

3 Results of the Simulations

Simulations are carried out using the reference values of the biophysical parameters listed in Tab.S1 (if not otherwise specified). Moreover, we set $N_S = 1000$, $b = 70\mu\text{m}$, $N_L = 16$, so that $L = (2b)N_L = 0.224\text{cm}$. We let $[t_{start}, t_{end}] = [0, 30]\text{days}$ and we use a space discretization parameter in the Macroscale simulations (see *SI methods*) $h = 1\mu\text{m}$ and a time discretization parameter $\Delta t = 1.5\text{h}$.

We first investigate the oxygen distribution throughout the scaffold thickness for an inlet oxygen tension $p_{O_2} = 20\%$. Fig. 5A shows the concentration profiles computed from the Macroscale model as a function of culture time. Each point on the reported curves represents the average concentration in the scaffold at different depths, identified by the layer number, 1=surface, 8=center. Results are shown in the static (no perfusion, dotted line) and interstitially perfused ($v_{in} = 50\mu\text{m/s}$, solid line) case. Fig. 5B shows the biomass thickness in the interstitially perfused regime at different layers. Difference Δ_h (positive values!) with respect to the biomass thickness in the static case is represented in the small inserted figure. Perfusion yields a higher biomass production, this phenomenon being much more evident for innermost layers, because fluid velocity favorably conveys a larger amount of nutrient to the deepest regions than in static conditions. However, diffusion barriers tend to smooth out the

differences for longer culture times, due to the net decrease of permeability (see also Fig. A1B) and -consequently- of fluid velocity magnitude caused by pore obstruction.

Referring from now on to the perfused case with $v_{in} = 50\mu\text{m/s}$, we investigate more in detail the statistical distribution of oxygen tension experienced by cells. The common practice in many bioreactor systems is simply to fix the inlet oxygen concentration at the saturation level c_{sat} . In reality, the situation is more complex, since cartilage cells are *in vivo* physiologically exposed to lower oxygen levels. Figs. 6A,B,C show the percentage of cells experiencing a certain range of oxygen tension at time $t = 5, 15, 30\text{days}$ parametrized as a function of the inlet concentration (bars represented in different colors). Simulations reveal that different inlet concentrations in the bioreactor result into significantly different distributions of oxygen levels throughout the construct and not only in a shift of the distribution. In particular, an inlet concentration equal to c_{sat} gives rise, as culture time advances, to increasingly more smoothed out distributions (“flattened bars”) of the number of cells receiving a certain level of oxygen, a point which might contrast with the target of obtaining uniform oxygen levels throughout the construct.

Eventually, we use the model to investigate the role of the metabolic regulation parameters and their interplay with scaffold matrix porosity. To this purpose, we first carry out a sensitivity study on effect of the rate of biomass synthesis k_{GAG} (for a fixed porosity $\Phi_0 = 0.8$). We assume for k_{GAG} a dependence on the oxygen tension experienced by the cells in the form a Gaussian distribution of mean μ and standard variation std (both expressed in oxygen tension values). Fig. 7A shows the (negative!) percentage variation of biomass thickness with respect to the case where k_{GAG} is set equal to the reference value $k_{GAG,ref}$. Variations are more important for innermost layer, which attain a lower nutrient concentration level. Different parameters for the Gaussian distribution are considered, in accordance with the indications obtained from results shown in Fig. 6. Then, we discuss the role of the parameter $m_{GAG,inh}$, which is a lumped representation of biomass production inhibition exerted on cells to maintain a certain homeostatic condition. Beforehand, we need to investigate more thoroughly the relation between biomass thickness, geometry and contact inhibition effects. Relation (14) reveals that for a given pore geometry and cellular post-initial conditions, there exists a threshold value m_{GAG}^* such that if $m_{GAG,inh} < m_{GAG}^*$, saturation occurs due to geometrical factors (pore obstruction) irrespective of biophysical homeostatic effects, otherwise biomass growth is limited by contact inhibition phenomena. Fig. 7B represents the (theoretical) value of $h_{b,max}$ obtained from Eq. (14) as a function of $m_{GAG,inh}$ parametrized on different initial porosities. Fig. 7C shows the biomass thickness computed by the multiscale model, as a function of time having set $t_{end} = 120\text{days}$ (steady state condition). Curves are parametrized for different values of design porosity Φ_0 and different values of $m_{GAG,inh}$ cho-

sen below and above the threshold value m_{GAG^*} . Simulations show that if $m_{GAG,inh} \leq m_{GAG^*}$, biomass growth is always controlled by inhibition effects, while if $m_{GAG,inh} > m_{GAG^*}$, after a first phase of the order of a few weeks, geometrical effects come into play, definitely limiting the increase of biomass thickness.

4 Discussion

Tissue Engineering is a strategy of Regenerative Medicine aimed at producing functional substitutes of tissues and organs, starting from donor cells cultivated in a controlled environment (bioreactor) capable of providing adequate conditions for cell viability and metabolism.

A main challenge in bioreactor optimization is the difficulty of establishing a relation between local biochemical and biomechanical processes and design parameters which, properly combined together, lead to achieve specified engineered tissue properties [11,12]. The usefulness of a more quantitative understanding of the phenomena occurring in bioreactor-based tissue regeneration is thus clear. In this perspective, the interaction with computational models may be profitably exploited to gain information which are often unaccessible to experimental measurements, for example the effect of a fine tuning of cellular metabolic mechanisms on biomass growth [20,19] in conjunction with a given scaffold matrix porosity.

There are numerous computational models of engineered tissue regeneration, many of them based on homogenized averaged approaches [28,14,6,36] or restricted to small portions of the domain including a selection of biophysical mechanisms with a strong emphasis on CFD [3,15,23].

The model presented in this study, which addresses in particular articular cartilage tissue engineered constructs, describes in a coupled framework nutrient (oxygen) transport and biomass growth. Despite in [7] an attempt was already made to couple phenomena occurring at different length scales, to our knowledge, the model proposed in this article is the first multiscale approach which allows to keep into account in a self-consistent manner the effect of barrier to the nutrient diffusive process caused by the pore obstruction due to biomass accumulation. The principle of scale separation is the central technique used to localize the problem at two representative scales: Macroscale and Microscale. This principle, in conjunction with biophysically consistent geometrical simplifications, allowed us to end up with a simulation tool capable of predicting bioreactor performance, even for long culture intervals, requiring at the same time a very limited computational effort.

What consequences can we draw from our model to improve bioreactor design? Biological studies indicate that *in vivo* cartilage is presumably exposed to “physiologically hypoxic” conditions with an oxygen tension ranging from 10% in the superficial layers to 1% in the deepest layers [17,8]. A widespread approach in TE practice is however to set a “hyper-physiological” (20%) oxygen tension at the device inlet, in order to prevent from nutrient shortage in the internal regions of the construct. With the present model, we were able to compute the local distribution of nutrient in the porous scaffold matrix resulting from a certain inlet oxygen tension. For a 20% inlet oxygen tension, computed oxygen levels (Fig. 5A) encompass a wide spectrum of values throughout the device thickness, ranging from nearly hyper-physiological conditions in the superficial layers to strongly hypoxia in the innermost layers [11,12,9]. We also investigated the spatial dependence of the oxygen distribution as a function of the inlet oxygen tension. Under hyperoxic inlet conditions, the distribution of cell percentage as a function of received oxygen tension is more smoothed out than under hypoxic conditions (Fig 6). Such a detailed knowledge (in contrast to a simpler read-out approach) of the oxygen tension experienced by cells can be used as a more sophisticated control parameter for cell’s metabolism than the sole oxygen inlet tension. This advanced concept is based on the evidence that a certain oxygen tension -which may, but not necessarily, be correspondent to the physiological levels - can be used to finely tune the *in vitro* synthesis of the various components of the ECM, cell proliferation and differentiation [8].

Direct perfusion bioreactors have been demonstrated to enhance nutrient convey, while applying hydrodynamic shear to cells, both conditions being believed to favour *in vitro* chondrogenesis [7]. With the model, we were able to quantify the role of perfusion on the local oxygen distribution in the construct. While the final level of oxygen is strongly influenced by diffusion barriers, the transient behavior to reach steady-state is significantly different from static culture conditions (Fig. 5A). As a result, in the same time interval, biomass production is strongly promoted by interstitial flow, this fact being much more evident in the innermost layers (Fig. 5B). As for the mechanical stimulus exerted on the cells by the fluid-dynamical field, it is known that moderate values of shear stress can enhance ECM production [33]. On the one side, shear stress is not experimentally accessible at the Microscale level, while existing CFD computational models at this scale do not account in a self-consistent manner for the presence of cells [34]. In the model we propose in this article, the shear stress information can be extracted either at the Macroscopic level as the Darcy stress, or estimated using the Microscopic radial velocity field at the fluid-biomass interface combined with a Coulomb-like friction law to obtain a tangential-like component needed to evaluate the shear stress at the fluid-biomass interface. This topic is, however, very delicate and needs further investigations.

The regulatory role of biomass production rate is another fundamental biophysical mechanism that we were able to explore. The idea was to test the evolution of biomass growth when not all the cells are subjected to the same “optimal” environmental conditions. Namely, for a given value of scaffold matrix porosity, a Gaussian distribution depending on the nutrient concentration is assumed for k_{GAG} and the resulting biomass thickness at the various scaffold levels is compared to that obtained taking k_{GAG} equal to the constant reference value $k_{GAG,ref}$ (Fig. 7A). The Gaussian distribution causes in general a reduction in biomass production, due to the fact that oxygen levels in the scaffold vary significantly. More specifically, the reduction is more important when the oxygen tension corresponding to the given central value μ of the Gaussian is experienced by a restricted percentage of cells. A much better performance is achieved when μ is close to a level of oxygenation that is more uniformly represented in the scaffold (case $\mu = 5\%$). Notice that this latter value of μ has been selected to reproduce the average oxygen tension experienced by chondrocytes *in vivo* [24]. For the same reason, given a certain value of μ , it turns out that tuning metabolic regulation around a narrow range of the concentration parameter (smaller *std*) is again more disadvantageous in terms of biomass production.

Eventually, reduction of biomass production due to cellular contact inhibition has been investigated in conjunction with different values of scaffold matrix porosity Φ_0 , a technologically relevant design parameter [34,23]. The maximum biomass production that can be obtained in a given scaffold pore depends, in a non easily predictable manner, on the interplay between contact effects and available void space. The theoretical results in Fig. 7B indicate that for each considered porosity, the threshold value m_{GAG^*} separates a regime where additional biomass formation is limited by contact effects ($m_{GAG,inh} \leq m_{GAG^*}$) from a saturation regime at which biomass production is only determined by pore obstruction ($m_{GAG,inh} > m_{GAG^*}$). Fig. 7C shows the computed temporal evolution of the biomass thickness in each layer for a very long culture process. Two classes of conclusions can be drawn. First, a higher accumulation of biomass is attained if $m_{GAG,inh} > m_{GAG^*}$, for both porosities, even when considering medium to short culture times (blue vs. red or magenta vs. green curves). Second, when the driving parameter is design porosity, a higher porosity produces more uniform results along the whole scaffold depth (spread of the curves along the y axis at a given time) due to diffusion barriers exerting a severe influence at later times (blue vs magenta or red vs. green curves).

Further aspects of the problem which deserve consideration for future investigation are: i) the inclusion of more detailed 3D effects while maintaining the computational cost at an affordable level. In this perspective, inhomogeneities in the (y, z) plane can be easily accounted for in our multiscale setting by assuming that the effective parameters are stochastic variables with average value given by the Micro-Macro transition proposed in the present model and

a certain variability which can be inferred from experimental data; ii) the inclusion of more detailed models of cell life-cycle, distinguishing between pools of cells in resting, proliferating and secreting states. In this perspective the change of state of a cell can be monitored via a system of integro-differential equation depending on age maturity parameters (see, *e.g.*, [2]).

5 Acknowledgments

This work was partially supported by Politecnico di Milano, under grant 5 per Mille Junior 2009 “Computational Models for Heterogeneous Media. Application to Micro Scale Analysis of Tissue-Engineered Constructs” CUPD41J10000490001 (to P.C. and R.S.).

References

- [1] Atala, A., Lanza, R., Thomson, J., Nerem, R.: Principles of regenerative medicine. Academic Press (2011)
- [2] Bernard, S., Pujo-Menjouet, L., Mackey, C.: Analysis of cell kinetics using a cell division marker: Mathematical modeling of experimental data. *Biophys J* **84**, 3414–3424 (2003)
- [3] Boschetti, F., Raimondi, M.T., Migliavacca, F., Dubini, G.: Prediction of the micro-fluid dynamic environment imposed to three-dimensional engineered cell systems in bioreactors. *J. Biomech.* **39**(3), 418–425 (2006)
- [4] Brezzi, F., Marini, L., Pietra, P.: Two-dimensional exponential fitting and applications to drift-diffusion models. *SIAM J. Numer. Anal.* **26**, 1342–1355 (1989)
- [5] Buschmann, M.D., Gluzband, Y.A., Grodzinsky, A.J., Kimura, J.H., Hunziker, E.B.: Chondrocytes in agarose culture synthesize a mechanically functional extracellular matrix. *J. Orthop. Res.* **10**(6), 745–758 (1992)
- [6] Chung, C., Chen, C., Chen, C., Tseng, C.: Enhancement of cell growth in tissue-engineering constructs under direct perfusion: Modeling and simulation. *Biotechnology and Bioengineering* **97**(6), 1603–1616 (2007)
- [7] Cioffi, M., Kueffer, J., Stroebel, S., Dubini, G., Martin, I., Wendt, D.: Computational evaluation of oxygen and shear stress distributions in 3d perfusion culture systems: Macro-scale and micro-structured models. *Journal of Biomechanics* **41**(14), 2918 – 2925 (2008)
- [8] Das, R., van Osch, G., Kreukniet, M., Oostra, J., Weinans, H., Jahr, H.: Effects of individual control of ph and hypoxia in chondrocyte culture. *Journal of Orthopaedic Research* **28**(4), 537–545 (2010). DOI 10.1002/jor.20994

- [9] Devarapalli, M., Lawrence, B., Sundararajan, V.: Modeling nutrient consumptions in large flow-through bioreactors for tissue engineering. *Biotechnol Bioeng* **103**(5), 1003–1015 (2009)
- [10] DiMicco, M., Sah, R.: Dependence of cartilage matrix composition on biosynthesis, diffusion, and reaction. *Transport Porous Med* **50**, 57–73 (2003)
- [11] Freed, L., Vunjak-Novakovic, G.: Tissue engineering bioreactors. In: R.P. Lanza, R. Langer, J. Vacanti (eds.) *Principles of tissue engineering*. Academic Press, San Diego (2000)
- [12] Freyria, A.M., Yang, Y., Chajra, H., Rousseau, C., Ronziere, M.C., Herbage, D., Haj, A.E.: Optimization of dynamic culture conditions: Effects on biosynthetic activities of chondrocytes grown in collagen sponges. *Tissue Engineering* **11**(5-6), 674–684 (2005)
- [13] Fu, X., Viskanta, R., Gore, J.: Prediction of effective thermal conductivity of cellular ceramics. *Int Comm Heat Mass Transfer* **25**(2), 151–160 (1998)
- [14] Galban, C.J., Locke, B.R.: Effects of spatial variation of cells and nutrient product concentrations coupled with product inhibition on cell growth in a polymer scaffold. *Biotechnology and Bioengineering* **64**(6), 633–643 (1999)
- [15] Galbusera, F., Cioffi, M., Raimondi, M.T., Pietrabissa, R.: Computational modelling of combined cell population dynamics and oxygen transport in engineered tissue subject to interstitial perfusion. *Computer Methods in Biomechanics and Biomedical Engineering* **10**(4), 279–287 (2007)
- [16] Gatti, E., Micheletti, S., Sacco, R.: A new Galerkin framework for the drift-diffusion equation in semiconductors. *East-West J. Numer. Math.* **6**(2), 101–135 (1998)
- [17] Grimshaw, M., Mason, R.: Modulation of bovine articular chondrocyte gene expression in vitro by oxygen tension. *Osteoarthritis and Cartilage* **9**, 357–364 (2001)
- [18] Hsu, C., Cheng, P.: Thermal dispersion in a porous medium. *Int. J. Heat Mass Transfer* **33**(8), 1587–1597 (1990)
- [19] Klein, T., Sah, R.: Modulation of depth-dependent properties in tissue-engineered cartilage with a semi-permeable membrane and perfusion: a continuum model of matrix metabolism and transport. *Biomech Model Mechanobiol* **6**, 21–32 (2007)
- [20] Knudson, W., Knudson, C.: Assembly of a chondrocyte-like pericellular matrix on non-chondrogenic cells. role of the cell surface hyaluronan receptors in the assembly of a pericellular matrix. *J Cell Sci* **99**(2), 227–235 (1991)
- [21] Landau, L., Lifshitz, E.: *Fluid Mechanics*. Pergamon Press (1959)
- [22] Langer, R., Vacanti, J.: Tissue engineering. *Science* **260**(5110), 920–926 (1993)

- [23] Lesman, A., Blinder, Y., Levenberg, S.: Modeling of flow-induced shear stress applied on 3D cellular scaffolds: implications for vascular tissue engineering. *Biotechnology and Bioengineering* **105**(3), 645–654 (2010)
- [24] Malda, J., Martens, D., Tramper, J., van Blitterswijk, C., Riesle, J.: Cartilage tissue engineering: Controversy in the effect of oxygen. *Critical Reviews in Biotechnology* **23**(3), 175–194 (2003)
- [25] Martin, I., Wendt, D., Heberer, M.: The role of bioreactors in tissue engineering. *Trends Biotechnol.* **22**(2), 80–86 (2004)
- [26] Nield, D., Bejan, A.: *Convection in Porous Media*. Springer-Verlag, New York (1998)
- [27] Nikolaev, N., Obradovic, B., Versteeg, H., Lemon, G., Williams, D.: A validated model of gag deposition, cell distribution, and growth of tissue engineered cartilage cultured in a rotating bioreactor. *Biotechnol Bioeng.* **105**(4), 842–853 (2010)
- [28] Obradovic, B., Carrier, R., Vunjak-Novakovic, G., Freed, L.E.: Gas exchange is essential for bioreactor cultivation of tissue engineered cartilage. *Biotechnol Bioeng.* **63**(2), 197–205 (1999)
- [29] Obradovic, B., Meldon, J.H., Freed, L.E., Vunjak-Novakovic, G.: Glycosaminoglycan deposition in engineered cartilage: Experiments and mathematical model. *AIChE J.* **46**, 1547–5905 (2000)
- [30] Potter, K., Butler, J., Adams, C., Fishbein, K., McFarland, E., Horton, W., Spencer, R.: Cartilage formation in a hollow fiber bioreactor studied by proton magnetic resonance microscopy. *Matrix Biol* **17**(7), 513 – 523 (1998)
- [31] Raimondi, M.: Engineered tissue as a model to study cell and tissue function from a biophysical perspective. *Current Drug Discovery Technologies* **3**(4), 245–68 (2006)
- [32] Raimondi, M., Candiani, G., Cabras, M., Cioffi, M., Laganà, K., Moretti, M., Pietrabissa, R.: Engineered cartilage constructs subject to very low regimens of interstitial perfusion. *Biorheology* **45**(3-4), 471–9 (2008)
- [33] Raimondi, M., Moretti, M., Cioffi, M., Giordano, C., Boschetti, F., Laganà, K., Pietrabissa, R.: The effect of hydrodynamic shear on 3D engineered chondrocyte systems subject to direct perfusion. *Biorheology* **43**(3-4), 215–22 (2006)
- [34] Raimondi, M.T., Boschetti, F., Migliavacca, F., Cioffi, M., Dubini, G.: Micro fluid dynamics in three-dimensional engineered cell systems in bioreactors. In: N. Ashammakhi, R.L. Reis (eds.) *Topics in Tissue Engineering*, vol. 2, chap. 9 (2005)
- [35] Roos, H.G., Stynes, M., Tobiska, L.: *Numerical methods for singularly perturbed differential equations*. Springer-Verlag, Berlin Heidelberg (1996)

- [36] Sacco, R., Causin, P., Zunino, P., Raimondi, M.T.: A multiphysics/multiscale 2D numerical simulation of scaffold-based cartilage regeneration under interstitial perfusion in a bioreactor. *Biomechanics and Modeling in Mechanobiology* pp. 1–13 (2010). URL <http://dx.doi.org/10.1007/s10237-010-0257-z>. 10.1007/s10237-010-0257-z
- [37] Schulz, R., Bader, A.: Cartilage tissue engineering and bioreactor systems for the cultivation and stimulation of chondrocytes. *Eur. Biophys. J.* **36**, 539–568 (2007)
- [38] Singh, H., Teoh, S., Low, H., Hutmacher, D.: Flow modelling within a scaffold under the influence of uni-axial and bi-axial bioreactor rotation. *Journal of Biotechnology* **119**(2), 181 – 196 (2005)
- [39] Vunjak-Novakovic, G., Freshney, I.: Culture of cells for tissue engineering. J. Wiley (2006)
- [40] Wendt, D., Stroebel, S., Jacob, M., John, G., Martin, I.: Uniform tissues engineered by seeding and culturing cells in 3d scaffolds under perfusion at defined oxygen tensions. *Biorheology* **53**, 481–488 (2006)
- [41] Whitaker, S.: The method of volume averaging. Theory and application of transport in porous media. Kluwer Academic Publishers (1999)
- [42] Wilson, C., Bonassar, L., Kohles, S.: Modelling the dynamic composition of engineered cartilage. *Arch Biochem Biophys* **408**(2), 246–254 (2002)
- [43] Wood, B.D., Quintard, M., Whitaker, S.: Calculation of effective diffusivities for biofilms and tissues. *Biotech. and Bioeng.* **77**(5), 495–514 (2002)
- [44] Wyatt, J., Mikulecky, D., DeSimone, J.: Network modelling of reaction-diffusion systems and their numerical solution using Spice. *Chem. Eng. Sci.* **35**(10), 2115–2127 (1980)

Appendix

A.1 Scale Transition

We detail in the following sections the computations required to perform scale transitions.

A.1.1 Micro–Macro Scale Transition

The Micro–Macro scale transition gives rise to effective coefficients that keep track, in the homogenized macroscopic model, of the microscale phenomena. Here below we detail the computation of the various coefficients.

Effective Porosity

The initial design porosity of the scaffold Φ_0 undergoes significant changes during culture time due to biomass growth. To compute the value of $\Phi_{(m,M)} = \Phi_{(m,M)}(\mathbf{x}_P, t)$ at each time level t and at the centroid of each pore $P \in \mathcal{P}_H$, we refer to the same simplified geometry proposed in [13], consisting of a cubic hollow box of side $2b$ and cubic hollow portion of side $2a$. The results obtained for this geometry provide a remarkably accurate approximation of the porosity of the cubic pore of Fig. 3B [13]

$$\Phi_{(m,M)} = \frac{6(b-a)(2(a-h_b))^2 + (2(a-h_b))^3}{(2b)^3}, \quad (\text{A1})$$

where $h_b = h_b(\mathbf{x}_P, t)$ is the biomass thickness predicted from Eq. (13) using the Microscale model in each pore $P \in \mathcal{P}_H$ and a is determined as the only admissible solution of the cubic equation $\zeta^3 - \frac{3}{2}\zeta^2 + \frac{\Phi_0}{2} = 0$, where $\zeta := a/b$, such that $0 \leq \zeta \leq 1$.

Effective Permeability

The homogenized permeability is computed from the Carman-Kozeny relation [26] as

$$K_{(m,M)}(\Phi_{(m,M)}) = K_i \frac{\Phi_{(m,M)}^3}{(1 - \Phi_{(m,M)})^2}. \quad (\text{A2})$$

The intrinsic permeability of the uncellularized scaffold K_i is determined by adapting the microscopic theory of dilute random array of spherical particles developed in [18] to the actual geometry of the scaffold, and is given by $K_i = d_K^2/150$, $d_K = 2b\sqrt[3]{6(1 - \Phi_0)/\pi}$ being the equivalent particle diameter of the

solid fraction of the scaffold pore. The effective permeability resulting from the numerical simulations and obtained using Eq. (A2) is shown in Fig. A1B as a function of scaffold depth.

Effective Diffusivity

Let us denote by $s = s(\mathbf{x}_P, t) = h_b(\mathbf{x}_P, t)/b$ the nondimensional thickness of the biomass layer of pore P . The homogenized diffusivity $D_{(m,M)} = D_{(m,M)}(\mathbf{x}_P, t)$ is computed generalizing the ideas of [13] to the multiphase (scaffold/biomass/fluid) system of the pore

$$\begin{aligned} \frac{D_{(m,M)}}{D_{fl}} &= ((1 - \zeta)/((\zeta - s)^2 + s(2\zeta - s)D_b/D_{fl}) \\ &+ (\zeta - s)/((1 - (s + 1 - \zeta)^2) + s(s + 2(1 - \zeta))D_b/D_{fl}) \quad (A3) \\ &+ s/((\zeta - s) + (1 - (1 - \zeta)^2 - (\zeta - s))D_b/D_{fl}))^{-1}, \end{aligned}$$

where we have supposed the scaffold to be impermeable to nutrient diffusion. The ratio $\frac{D_{(m,M)}}{D_{fl}}$ resulting from the numerical simulations and obtained using Eq. (A3) is shown in Fig. A1A as a function of scaffold depth.

Effective Consumption Rate

To characterize the effective consumption rate $R_{(m,M)}$, we require that

$$\int_{V_{\text{cub}}} R_{(m,M)} dV = \int_{V_b} R dV.$$

The above bridging condition states that oxygen consumption per unit time referred to the volume of the cubic pore is equal to the consumption per unit time occurring in the biomass layer at the microscopic scale, and yields

$$R_{(m,M)} = \frac{\Psi_{\text{max}} N_{\text{cells}}^{\text{tot}}}{V_{\text{cub}}}. \quad (A4)$$

A.1.2 Macro–Micro Scale Transition

The function $c_{(M,m)} = c_{(M,m)}(\mathbf{x}_P, t)$ is defined at each time t as the average macroscopic concentration of each pore $P \in \mathcal{P}_H$, and can be numerically computed using Eq. (A9).

A.2 Problem discretization

We detail in the following sections the discretization schemes used to solve the coupled Micro-Macro scale problem.

A.2.1 Solution of the Microscale Problem at Step A.1

The nutrient problem in Step A.1 is beforehand linearized by replacing in the biomass domain the consumption term $Q(c_m)$ with $\tilde{Q}(c_m) = \chi^n c_m$, where $\chi^n = -\frac{\Psi_{max}}{K_{1/2} + c_m^n} \xi_{cells}^n$. At each time level t_{n+1} , $n = 0, \dots, N_t - 1$, the solution of the linearized Microscale nutrient problem is then the following piecewise smooth function $c_m : \Omega_{m,fl}^n \cup \Omega_{m,b}^n \rightarrow \mathbb{R}$:

$$c_m^{n+1}(r) = \begin{cases} c_{(M,m)}^n & \text{for } r \in (0, r_b^n), \\ \kappa c_{(M,m)}^n \frac{F(r)}{F(r_b^n)} & \text{for } r \in (r_b^n, r_w), \end{cases} \quad (\text{A5})$$

where F is the shape function defined as

$$F(r) = \frac{1}{r} \left(\left(r_w \sqrt{\frac{\chi^n}{D_b}} + 1 \right) \exp \left\{ (r - r_w) \sqrt{\frac{\chi^n}{D_b}} \right\} + \left(r_w \sqrt{\frac{\chi^n}{D_b}} - 1 \right) \exp \left\{ - (r - r_w) \sqrt{\frac{\chi^n}{D_b}} \right\} \right).$$

Having determined the new biomass position, one can compute the constant α that uniquely specifies the admissible fluid velocity in the spherical pore by enforcing the flux continuity condition (10), to obtain

$$\alpha^{n+1} = -\kappa D_b \frac{(r_b^{n+1})^2 F'(r_b^{n+1})}{c_{(M,m)}^n F(r_b^{n+1})}. \quad (\text{A6})$$

A.2.2 Solution of the Microscale Problem at Step A.2

In order to compute the new biomass thickness h_b^{n+1} from Eq. (13), we solve analytically the linearized version of problem (11) obtained using for $c_{(M,m)}$ the newest available value $c_{(M,m)}^{n+1}$ computed from point A.1 and for ξ_{cells} the value $V_b(t_n)$ computed at the previous time level.

A.2.3 Solution of the Macroscale Problem at Step C

Let \mathcal{T}_h be a uniform partition of $[0, \ell]$ into N_h subintervals T of size $h < H$ and $c_{M,h}$, $J_{M,h}$ be the numerical approximations of c_M and J_M , respectively, with $c_{M,h}$ piecewise linear continuous and $J_{M,h}$ piecewise constant over \mathcal{T}_h . At time level t_{n+1} , the first step is to compute the constant value of the Darcy velocity, solution of problem (16)

$$v_M^{n+1} = v_{in} \frac{\mathcal{H}(K(\Phi^{n+1})/\Phi^{n+1})}{K(\Phi_0)/\Phi_0} \quad \text{in } \mathcal{T}_h, \quad (\text{A7})$$

$\mathcal{H}(f)$ being the *harmonic average* of the function f over $[0, \ell]$, defined as $\mathcal{H}(f) := (\int_0^\ell f^{-1}(s)ds/\ell)^{-1}$. Then, the next step consists of solving the nutrient problem (15) using the velocity computed from (A7) and using internal fixed point iterations to deal with the non-linear consumption term. The Galerkin approximation of (15) with the exponentially fitted finite element method proposed and studied in [4,16] is then carried out. This scheme enjoys several interesting properties. The function $c_{M,h}$ satisfies a discrete maximum principle irrespective of the value of the local Péclet number [35]. This property prevents the numerical scheme from the onset of spurious oscillations if the fluid velocity becomes large, and ensures that the discrete Macroscale nutrient concentration is strictly positive and uniformly bounded by c_0 . The function $J_{M,h}$ satisfies at each (internal) mesh node x_i separating elements T_i^- and T_i^+ the following discrete conservation law

$$J_{M,h}^+ - J_{M,h}^- = \tilde{Q}_M(c_{M,i})h. \quad (\text{A8})$$

Multiplying both sides of (A8) by the cross-section pore area in the transverse (y, z) plane, we obtain the “mass flux” equivalent of a Kirchhoff current balance with respect to node x_i (see also [44] for a discussion of the electrical analogue of reaction–diffusion systems). The average concentration required by Macro-Microscale bridging can be computed as

$$c_{(M,m)}^{n+1}(\mathbf{x}_P) = H^{-1} \sum_{T \in P} \int_T c_{M,h}^{n+1} dx. \quad (\text{A9})$$

Table 1
Biophysical parameters

Capital letters		Small letters			Greek letters			
symbol	value	units	symbol	value	units	symbol	value	units
D_b	2.2×10^{-5}	cm^2s^{-1}	c_{sat}	6.4×10^{-6}	g cm^{-3}	κ	0.5	–
D_{fl}	3.2×10^{-5}	cm^2s^{-1}	h_0	5×10^{-4}	cm	μ_{fl}	8.26×10^{-3}	$\text{g cm}^{-1} \text{s}^{-1}$
E	20	–	$k_{GAG,ref}$	2.38	$\%_{\text{ww}} (\text{day mM (cell/mm}^3))^{-1}$	ρ_{fl}	1	g cm^{-3}
$K_{1/2}$	1.92×10^{-7}	g cm^{-3}	$m_{GAG,inh}$	3.5	$\%_{\text{ww}}$	Φ_0	0.8	–
N_{cells}^{tot}	300	–	v_{in}	50×10^{-4}	cm s^{-1}	Ψ_{max}	1.28×10^{-16}	$\text{g}(\text{cells s})^{-1}$

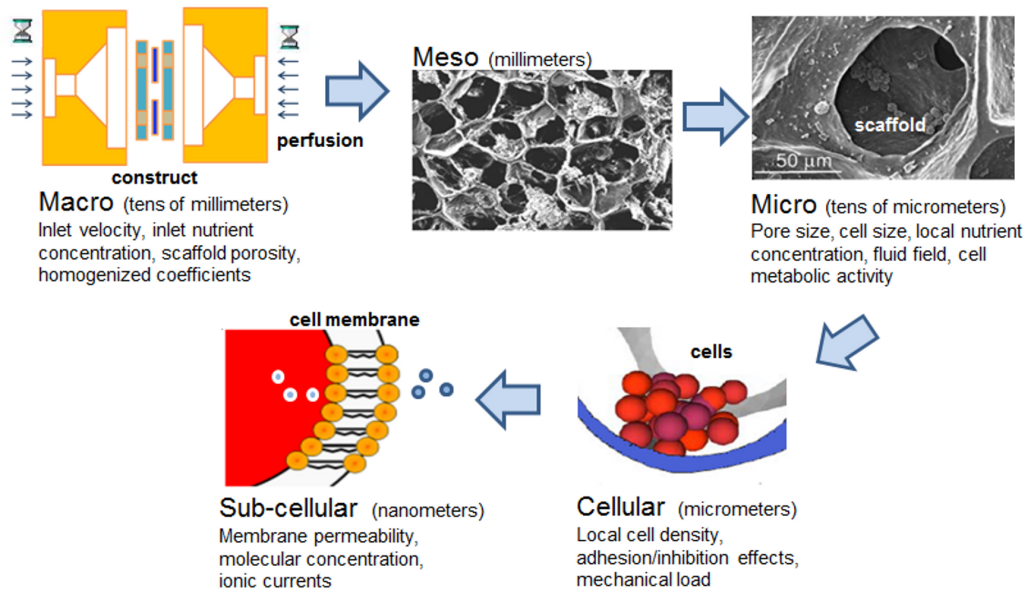


Fig. 1. Multiple scale in TE mathematical models. The figure shows a selection of scales relevant to biophysical phenomena occurring in engineered tissue regeneration, along with the corresponding significant biotechnological parameters. Macroscale: it is the scale at which the perfused scaffold is treated as a continuum and at which the Bioengineer sets the control parameters (inlet velocity, scaffold porosity); Mesoscale: corresponds to a collection of a few functional units of the scaffold; Microscale: it is the scale of the single functional unit (here, the pore) of the polymeric scaffold, of nominal diameter of the order of $100\mu\text{m}$; Cellular scale cells should be treated as discrete entities and phenomena like adhesion and contact forces should be accounted for; Sub-cellular scale: accounts for all the mass transport and reaction processes that occur at the single cell membrane level.

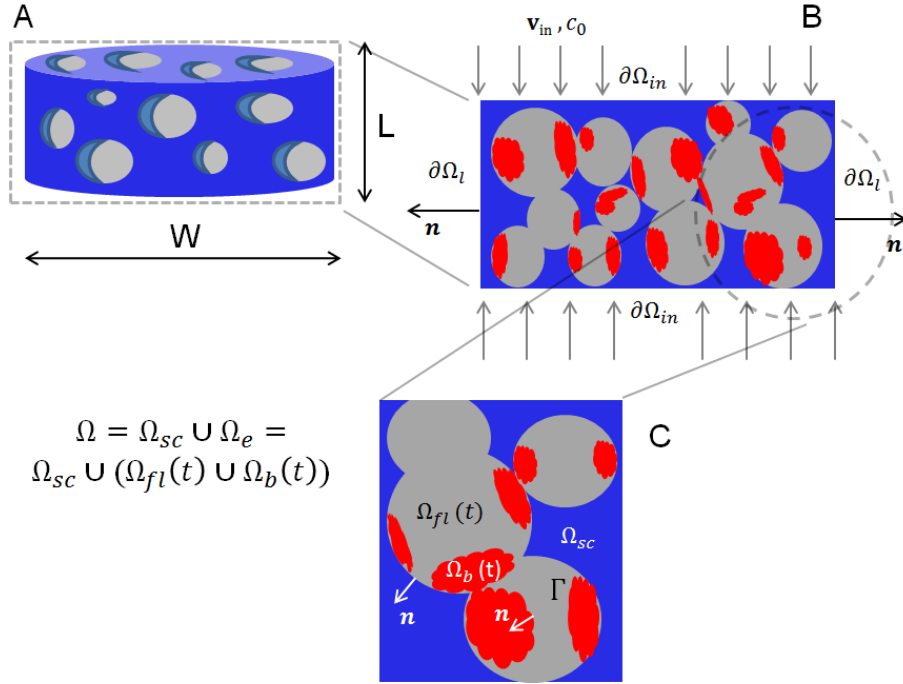


Fig. 2. Geometry and notation. A. 3D porous construct. B. 2D cross-section of the construct, with length L and thickness W . C. Zoomed view of the multiphase composition of the construct. We denote by Ω the bioreactor domain, with boundary $\partial\Omega = \partial\Omega_{in} \cup \partial\Omega_l$. The domain Ω is composed by the time-invariant subdomain $\Omega_{sc} = \Omega_{sc}(t)$, representing the scaffold, and by its complement $\Omega_e = \Omega_e(t)$. This latter subdomain is, in turn, composed of the time dependent fluid portion $\Omega_{fl} = \Omega_{fl}(t)$ and the biomass portion $\Omega_b = \Omega_b(t)$, both of which may be, in general, composed by the union of unconnected domains of complex shape. The interface separating Ω_{fl} and Ω_b is denoted by Γ . Moreover, \mathbf{n} indicates the unit normal vector on $\partial\Omega$ and on each material interface.

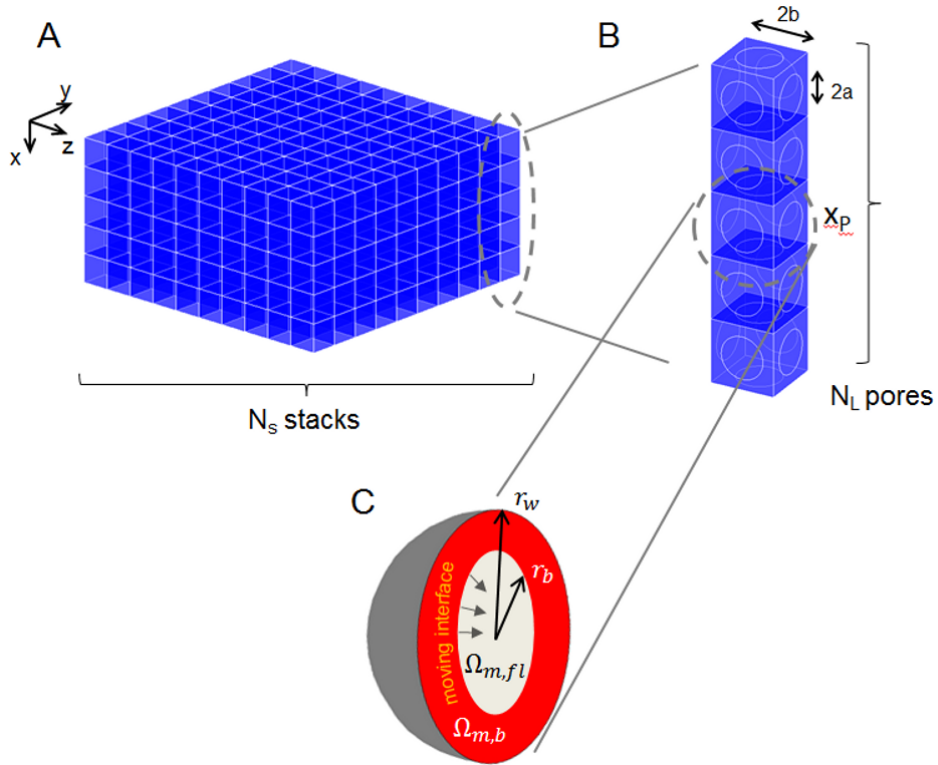


Fig. 3. Idealized geometry. A. The bioreactor construct is composed by a regular mosaic of “cubic pores” which represent the functional sub–units. The cubic pores are organized in N_S stacks. B. Stack of pores. Each stack is partitioned into N_L pores and is aligned along the x axis, along which the coordinate of the centroid of the pore P is denoted by x_P . C. Spherical pore. The origin of the coordinate system is located at the pore center, the fluid biomass interface at $r_b = r_b(t)$ and the pore wall at $r = r_w$, respectively. Biomass is supposed to uniformly grow inwardly along the radial direction.

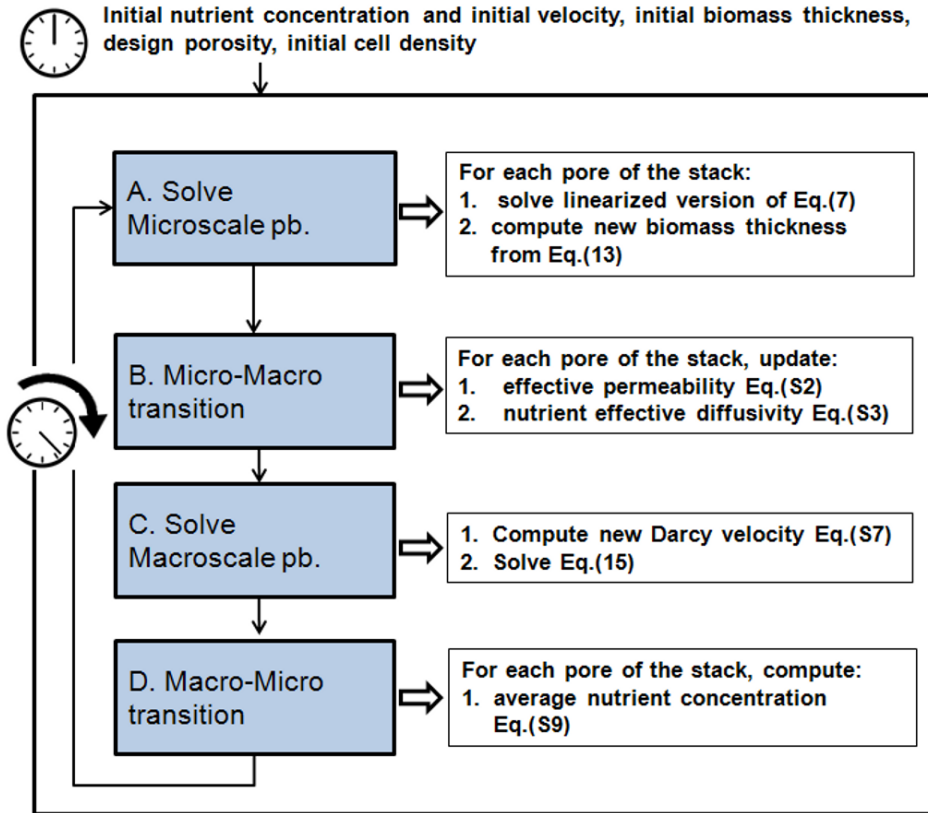


Fig. 4. Computational Multiscale staggered algorithm. Details of the discretization of each sub-problem are given in the *SI* text. The initial distribution of nutrient concentration along the scaffold depth is determined by a first run (outside the time loop) of the Macroscale model. Notice that the solution of the Microscale problems at Step A. and Scale transition computations at Steps B. and D. can be carried out in parallel over the stack for each representative pore of the layer. Macroscale computations are serial, but their cost is negligible.

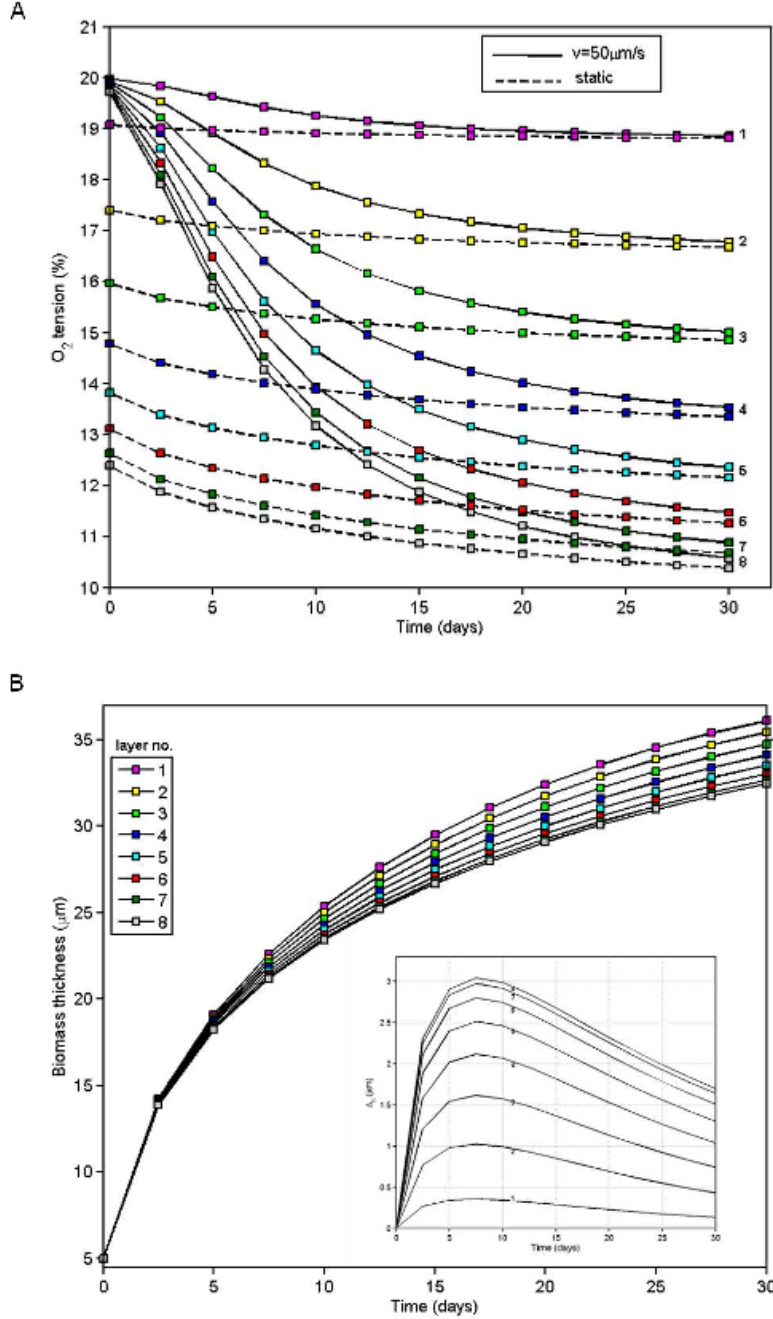


Fig. 5. Effect of perfusion (solid line $v_{in} = 50 \mu\text{m/s}^{-1}$, dashed line static condition $v_{in} = 0$) as a function of time at different scaffold depths (layer 1=surface, 8=center of the construct) with $c_0 = c_{sat}$. A. Macroscale nutrient concentration. B. Evolution of biomass thickness and difference in thickness with respect to static conditions (boxed insert). Results clearly indicate that perfusion enhances nutrient availability during the culture process, despite the fact that contact inhibition and pore obstruction give rise to a natural saturation of biomass growth. Perfusion yields a substantially higher biomass production, this phenomenon being much more evident for internal layers because fluid velocity favorably conveys a larger amount of nutrient to the deepest regions than in static conditions.

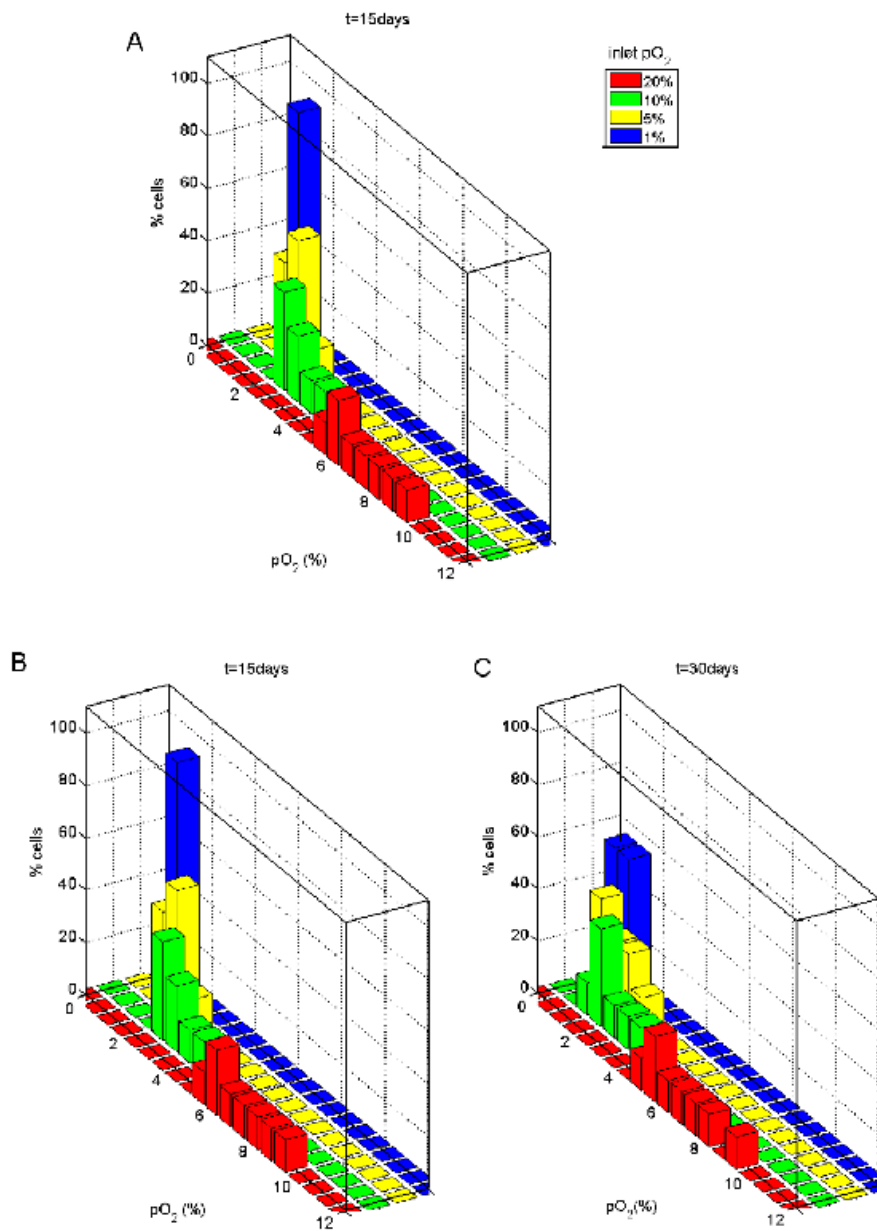


Fig. 6. Percentage of cells in the construct experiencing a certain oxygen tension as a function of the inlet oxygen tensions (20% “hyperoxic” condition, 5 – 10% “physiological hypoxic” conditions, 1% “strongly hypoxic” condition), computed at culture times 5, 15, 30 days. Results show the common trend of a decrease in the oxygen tension experienced by cells as time increases. The distribution of cell percentages is more peaked under hypoxic to strongly hypoxic conditions, while it becomes more flattened under hyperoxic conditions. These results give indications to the Bioengineer of which inlet oxygen tension should be applied in order to guarantee a desired range of nutrient availability over all the construct.

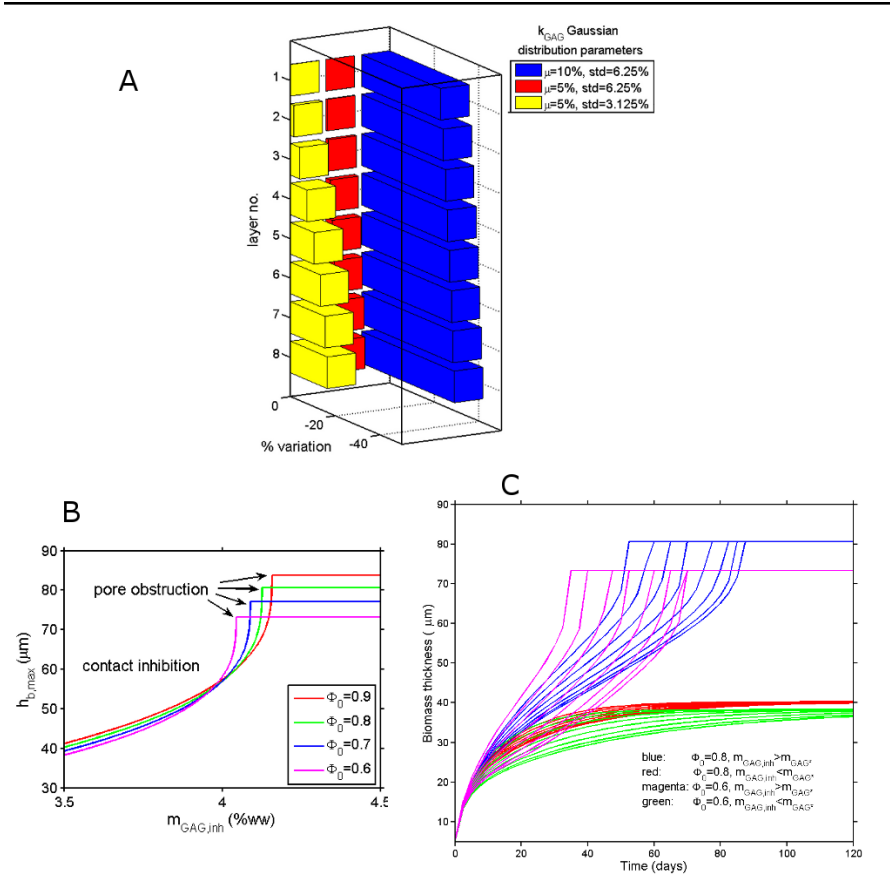


Fig. 7. Sensitivity analysis. A. Effect of variation of the rate of biomass production. The dependence of the rate of matrix synthesis k_{GAG} on the local oxygen concentration c is assumed to be a Gaussian distribution $k_{GAG}(c) = Ae^{-(c-\mu)^2/(2std^2)}$, where $A = k_{GAG,ref}$ is the maximal amplitude, μ is the average and std the standard deviation (all expressed in oxygen tension units). Different parameters for the Gaussian distribution are considered, in accordance with the indications obtained from results shown in Fig. 6. Percentage variation (negative values!) of the biomass thickness obtained at $t = 30$ days is compared to that obtained using the constant value $k_{GAG,ref}$, as a function of the layer number (1=surface, 8=center of the construct). Simulations suggest a scenario for which a metabolic optimization on relatively high oxygen levels ($\mu = 10\%$) is disadvantageous, since these levels cannot be attained uniformly in the scaffold due to diffusion barriers. In the case $\mu = 5\%$, if a “too narrow metabolic regulation” is displayed by cells ($std = 3.125\%$), again biomass secretion could be disadvantaged. B. Maximum biomass thickness. The maximum biomass production depends on the interplay between inhibition effects and available void space. To investigate this complex biophysical picture, we let the saturation GAG level $m_{GAG,inh}$ to vary within a physiological interval and compute the theoretical value of $h_{b,max}$ according to Eq. (13) using as a parameter the scaffold porosity. The threshold value m_{GAG}^* is identified on each curve by the abrupt change of slope. The regimes biomass formation limited by contact inhibition ($m_{GAG,inh} \leq m_{GAG}^*$) or geometric factors ($m_{GAG,inh} > m_{GAG}^*$) can be clearly distinguished. C. Combined effect of contact inhibition, scaffold porosity and time evolution of biomass. Computed biomass produced in each layer of the scaffold is shown as a function of time till long culture periods (120days) for two different values of design scaffold porosity Φ_0 and for the two cases $m_{GAG,inh} \lesseqgtr m_{GAG}^*$. Most superficial layers correspond in all cases to the uppermost curve of each family. Two classes of conclusions can be drawn from the graph. First, a higher accumulation of biomass is attained if $m_{GAG,inh} > m_{GAG}^*$, for both porosities, even when considering medium to short culture times (blue vs. red or magenta vs. green curves). Second, when the driving parameter is design porosity, a higher porosity produces more uniform results along the whole scaffold depth (spread of the curves along the y axis at a given time) due to diffusion barriers exerting a severe influence at later times (blue vs. magenta or red vs. green curves).

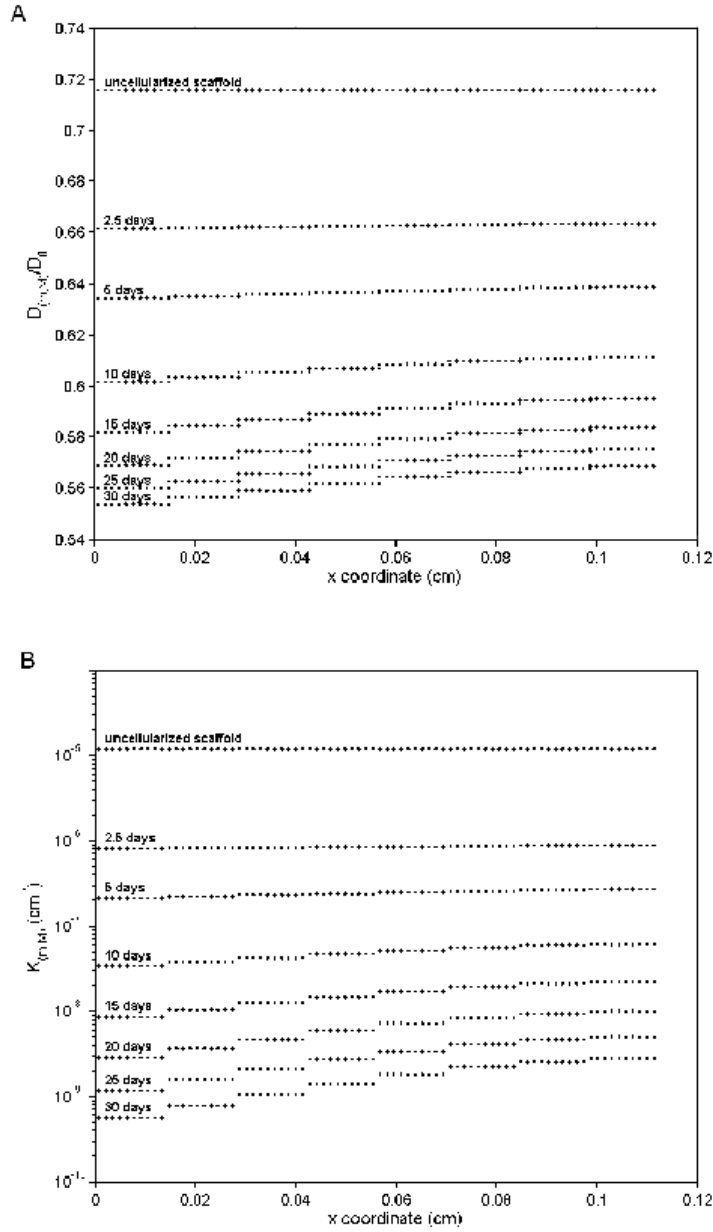


Fig. A1. Effective parameters computed at different culture times for a design porosity $\Phi_0 = 0.8$. A. Effective diffusivity normalized to clear fluid diffusivity computed from Eq. (A3). Notice that even in the uncellularized condition, the obstruction to diffusion exerted by the presence of the scaffold phase causes a reduction of 25% of the diffusivity. The presence of the growing biomass enhances such a reduction up to 50%. The reduction is not uniform along the scaffold depth due to the different evolution of biomass growth. B. Effective permeability computed from Eq. (A2). Logarithmic scale is used on the y axis to emphasize the significant variation (two orders of magnitude) of the permeability. Analogous comments as in A. apply also to this case.